Indian Journal of Chemistry
Vol. 63, June 2024, pp. 604-612
DOI: 10.56042/ijc.v63i6.9533

Harnessing the polarizability of capping ligands for enhancing the intensity of hypersensitive electric dipole transition in Eu^{3+} doped CaF_2 nanoparticles

Ngasepam Bhogenjit Singh & Thiyam David Singh*
Department of Chemistry, National Institute of Technology Manipur, Langol 795 004, India
E-mail: davidthiyam@yahoo.co.in

Received 13 March 2024; accepted (revised) 25 April 2024

The enhancement of intensity of the hypersensitive $^5D_0 \rightarrow {}^7F_2$ transition in Eu^{3+} doped CaF_2 nanoparticles (NPs) by exploitation of polarizability of the stabilizing ligands (ethylene glycol (EG), citrate (TSC) and EDTA) is reported. The correlation between the asymmetric ratio, R $\{I(^5D_0 \rightarrow {}^7F_2)/I(^5D_0 \rightarrow {}^7F_1)\}$ of the transition with the nature of the capping ligands is studied by determining Judd-Ofelt intensity parameter (Ω_2), radiative transition probability (A) and average lifetime (τ). R is maximum for EDTA capped NPs followed by TSC and EG capped NPs. Bi-exponential fitting of the decay curves indicate the contribution of Eu^{3+} in the grain boundary to the R value is maximum for EDTA stabilized NPs. Cytotoxicity studies on epithelial human breast cancer cell (MDA 231) and RAW 264.7 cells suggested biocompatibility of 75% up to a maximum concentration 250 µg/mL. These characteristics demonstrate the potential of employing these synthesized nanoparticles in the fields of optical devices, as well as in bioimaging.

Keywords: Calcium fluoride nanoparticles, Hypersensitive transition, Intensity enhancement, Stabilizing ligands, Biocompatibility

Rare-earth-based materials are versatile enough for ranges of potential applications in the fields of optoelectronics and biomedicines[1,2]. Among the lanthanides, Eu(III) based complexes and nanoparticles (NPs) are extensively investigated as luminescent materials for emission devices, security media, fluorescent bioprobes, biolabelling, *etc*.[3,4] Moreover, Eu(III) ion is used as an optical probe for determining the site symmetry of host compound as compared to other Ln(III) ions utilizing the hypersensitive nature of the electric dipole transition $^5D_0 \rightarrow {}^7F_J$ (J = 2, 4, 6) to the local symmetry with respect to the magnetic dipole transition $^5D_0 \rightarrow {}^7F_1$[5,6]. The emission corresponding to $^5D_0 \rightarrow {}^7F_2$ transition that appear around 615 nm has relatively large luminosity factor in the red region and its sharpness make a remarkable contribution on the properties of white LED by allowing easy adjustment of the spectrum[3]. This particular transition also extends its importance in the application of bioimaging where the purity of red colour is of utmost importance for reducing autofluorescence from living tissue for a better resolution of the image in addition to a lower photo-toxicity[7]. Enhancement of the intensity of the electric dipole transition of Eu (III) ion were witnessed in many reports where attempts were made by forming complexes with unsymmetrical ligands, in compounds/complexes with highly polarisable polyanions/ligands, increasing the dopant concentration sacrificing the crystallinity of the host NPs to the increasing defects leading to the decrease in local symmetry, *etc*.[3,8,9] But the drawbacks of complexes against inorganic based NPs doped with Eu (III) ions for use in emission devices as well as bioimaging[10,11] led to the incessant search for an improved combination of the emitting species and host medium that possesses properties demand by the applications. For such applications, inorganic fluoride host compound like CaF_2 serves as a suitable candidate as it possesses high transparency ranging from UV to IR regions that combines with a low phonon energy reducing the non-radiative transition probability of the emitting species resulting in higher quantum efficiency[12,13]. For intervention to biological systems also, CaF_2 having an optically isotropic fluorite structure evolves as an efficient candidate due to its non-toxicity, non-hygroscopic, high stability and biocompatibility[14]. The stability and biocompatibility of the NPs is achieved by proper selection of capping ligands. Besides tailoring the size and directing the morphology of the synthesized NPs, properties like photoluminescence and cell uptake capacity also rely

on the stabilizing ligands[15-21]. But it would be a great accomplishment if only changing the capping ligand could enhance the transition probability of the electric dipole transition of the Eu(III) ions increasing the purity of the red colour of the spectrum without compromising the properties of the host matrix. Considering these significances, the role of common biocompatible stabilizing ligands like ethylene glycol (EG), citrate and ethylenediamminetetraacetate (EDTA)[22-26] which also allows easy surface modification for attaining multifunctionality needs to be investigated.

In this report, the effect of the three surface capping ligands – EG, citrate and EDTA in triggering the transition probability of the $^5D_0 \rightarrow {}^7F_2$ transition of Eu (III) is studied in red emitting Eu^{3+} doped CaF_2 NPs. For this purpose, 3 at% Eu^{3+} doped CaF_2 NPs (CaF_2:3Eu) were synthesized following a simple colloidal precipitation technique using the three ligands employing similar reaction conditions. The Judd-Ofelt intensity parameters, radiative transition probabilities along with fluorescence lifetimes were used to correlate the observed luminescence properties of each NPs to the stabilizing ligand. Biocompatibility of the synthesized NPs was assessed using epithelial human breast cancer cell (MDA 231) and RAW 264.7 cells in conjunction with binding studies with bovine serum albumin (BSA).

Experimental Section

Materials

Calcium carbonate, $CaCO_3$ (99.0%), europium (III) oxide, Eu_2O_3 (99.99%), trisodium citrate dihydrate, $C_6H_5Na_3O_7.2H_2O$ (TSC), ethylenediamminetetraacetic acid trisodium salt hydrate, $C_{10}H_{13}N_2Na_3O_8.xH_2O$ (95%) and ammonium fluoride, NH_4F (99.99%) were acquired from Sigma Aldrich and ethylene glycol and hydrochloric acid from Merck. All the reagents and chemicals were used as received. All throughout the experiment, deionised water was used.

Synthesis

All the NPs were synthesized using a 0.2 M aqueous stock solution of 3 at% Eu^{3+} in Ca^{2+} which is prepared by digesting stoichiometric amount of calcium carbonate, $CaCO_3$ (1.94174 g) and europium (III) oxide, Eu_2O_3 (0.10558 g) using concentrated HCL (5 mL) with further removal of the acid by repeated evaporation and dilution process. All the ligand concentrations were optimized beforehand.

A mixture of aqueous TSC (0.2941g in 20 mL H_2O) with 25 mL stock solution in a 100 mL three-neck round bottomed flask was heated in an oil bath with constant stirring. When the temperature reached 40°C, 0.37781 g of NH_4F dissolved in minimum amount of water was added when a dense white precipitate appeared indicating the formation of CaF_2 NPs doped with Eu^{3+}. Within 40 min, the reaction temperature was raised to 100°C. After stirring for 90 min, the reaction mixture was removed from the bath and cooled to RT. The same steps were followed for synthesizing EDTA and EG capped NPs by taking 0.35819 g EDTA while for EG, the capping agent was made the reaction medium. All the reactions took place by maintaining a total volume of 50 mL. Excess ligands and precipitating agents were removed by centrifugation at 10000 rpm with further redispersing in water. The process was repeated three times. NPs samples CF_TSC, CF_EDTA, and CF_EG capped with TSC, EDTA and EG respectively, were obtained.

Biological Studies

MTT Assay

The biocompatibility of the synthesized NPs was assessed by studying the *in vitro* cytotoxicity at Institute of Bioresources and Sustainable Development, Imphal, India using MDA 231(epithelial human breast cancer) and normal Raw 264.7 cell lines procured from National Centre for Cell Sciences, Pune, India by the method of MTT assay. The cells were cultured in a complete medium of RPMI 1640 + FBS + fungizone + penstrep at 37°C in a 5% CO_2 atmosphere.

The cells were seeded in a 96-well plate at an approximate density of 1×10^4/100 µL/well incubating at 37°C with a 5% CO_2 concentration for 24 h in a CO_2 incubator. The cells were then treated with varying concentrations of NPs samples (15.62, 31.25, 62.5, 125, 250, 500 and 1000 µg/mL). After 24 h the culture medium was removed and washed with PBS after which the cells were treated with 100 µL of 5 mg/mL MTT solution, diluted with culture medium in each well for 4 h. With the help of an inverted microscope, the condition of the cells and the formation of formazone crystals were examined whence 100 µL of stopper solution (10% SDS solution in 0.1N HCl) was added to each well and further incubated in dark overnight. The absorbance of each well was recorded using the SpectralMax M5e multimode microplate reader at 595 nm. The cell viability was then estimated as [(absorbance value of the test divided by absorbance of control) × 100].

BSA Binding Study

The binding ability of the synthesized NPs to the serum albumin which acts as a carrier in the blood was studied by taking bovine serum albumin (BSA) which is homologous to human serum albumin (HSA)[27]. To 200 µL of 3×10^{-5} M BSA solution, 2 mL Tris-HCl buffer solution was added and the emission spectrum of the mixture was recorded using Hitachi F-7000 fluorescence spectrophotometer. The emission spectra of the mixture were further recorded with the addition of increasing amount of NPs samples where the increased took place at an increment of 2.5 µL of 10 mg mL^{-1} sample solution. The binding constants of the different NPs samples with BSA were determined using equation (3).

Characterization

The synthesized NPs were characterized through XRD, FTIR, TEM, EDS and photoluminescence studies. The detail methods of analyses using different instruments were same as reported[28].

Results and Discussion

The X-ray diffraction patterns of the synthesized CaF_2:3Eu NPs with different ligands in comparison with the reference pattern (ICDD PDF 00-035-0816) are shown in Fig. 1. The recorded patterns conformed to the reference pattern having cubic phase of CaF_2 with a fluorite structure and a space group *Fm-3m*. The observed peaks can be indexed to (111), (220), (311), (400), (331) and (422) diffraction planes and the absence of any other peaks characteristics of citrates and EDTA complexes of calcium and europium signifies the phase purity of the samples. The reported lattice parameter and unit cell volume for the reference (PDF 00-035-0816) are a = 5.463 Å and V = 163.04 $Å^3$ respectively. For the synthesized NPs, the calculated lattice parameters are 5.468, 5.467 and 5.467 Å for CF_EG, CF_TSC and CF_EDTA respectively, while their respective unit cell volumes are 163.51, 163.39 and 163.39 $Å^3$. The incorporation of Eu^{3+} ions at Ca^{2+} sites and the subsequent formation of charge compensatory interstitial F^- ions led to the introduction of lattice defects, the effect of which is manifested in the diffraction patterns.

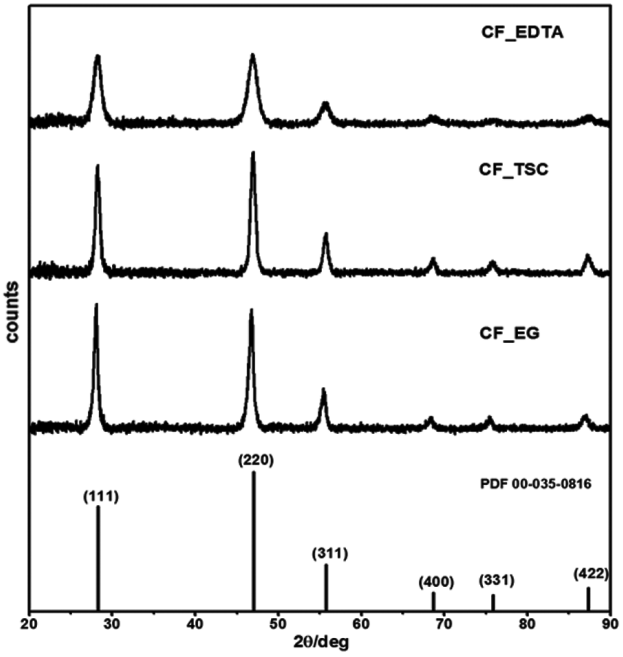

Fig. 1 — XRD patterns of the 3 at% Eu(III) doped CaF_2 NPs capped with a) EDTA (CF_EDTA), b) TSC (CF_TSC) and c) Ethylene glycol (CF_EG) with reference pattern (00-035-0816)

Williamson-Hall analysis of the diffraction patterns shows the combined effects of crystallite size and strain in the broadening of the peaks. A perusal of crystallite sizes and strains (Table 1) of the NP samples indicate CF_EDTA has the smallest size with maximum lattice defects leading to the largest value of full width at half maximum (FWHM) with smallest intensity . The ability of EDTA to form highly stable complex with Ca^{2+} (1.98×10^8 M^{-1}) (Ref. 29) hinders the uniform growth of crystal thereby acquiring maximum defects while terminating the growth process within a short span of time resulting into the formation of highly monodispersed particles with increased strain.

The TEM images of the synthesized NPs (Fig. 2) indicate that CF_EDTA have cuboidal morphology with a narrow size distribution (Table 1) as evident from the TEM distribution profiles. CF_TSC and CF_EG have quasi-spherical shapes with broader distribution profiles. The calculated NPs sizes were in agreement with those obtained (Table 1) from TEM analysis. The crystalline nature of the synthesized NPs samples is confirmed from the SAED images (inset Fig. 2(a-c)) where the various bright dotted rings indicate different planes of diffraction of CaF_2 crystal. The lattice planes in the HRTEM images (inset Fig. 2(a-c)) indicate that preferred growth of the crystallite takes place along (111) plane. EDX spectra

Table 1 — Crystallite sizes, strains and TEM sizes of CaF_2:3Eu NPs stabilized by EDTA, TSC and EG

Samples	Williamson-Hall analysis		TEM analysis
	Crystallite size, t (nm)	Strain, $\varepsilon/10^{-4}$	size, d (nm)
CF_EDTA	5.82	-24.9	5.42±0.06
CF_TSC	12.00	-0.74	10.81±0.13
CF_EG	12.41	-0.116	10.19±0.25

confirm the incorporation of Eu^{3+} in the CaF_2 matrix (Fig. 3) for all the samples.

FT-IR spectra (Fig. 4) of all the synthesized NP samples along with the pure ligands confirmed the conjugation of the respective stabilizing ligands with Ca onto the NP surface. The observed absorption bands of all the samples were consistent with previous report[28].

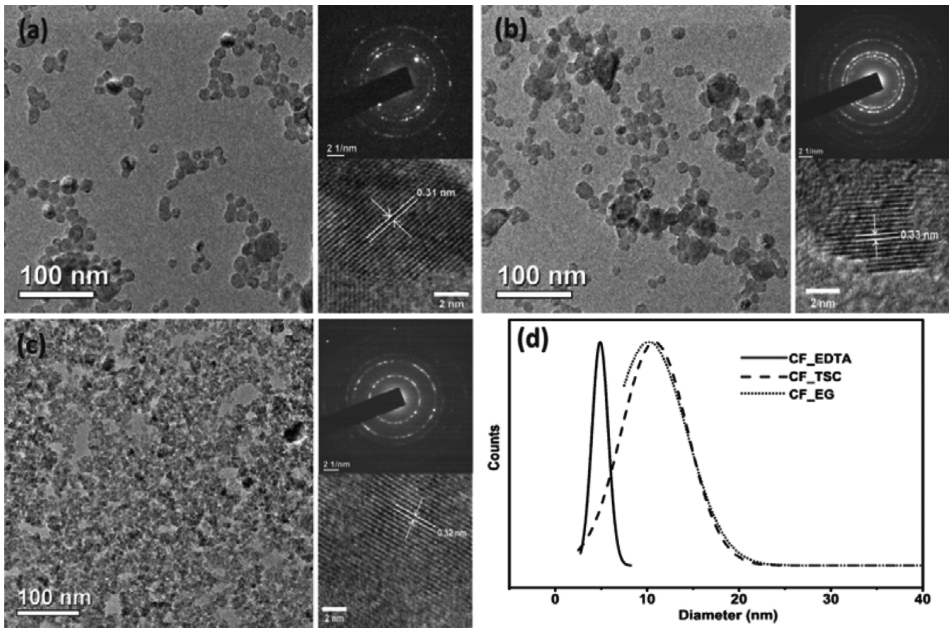

Fig. 2 — EM images, SAED patterns, HRTEM images and interplanar spacings of (a) CF_EG (b) CF_TSC, (c) CF_EDTA samples and the corresponding (d) size distributions obtained from TEM images

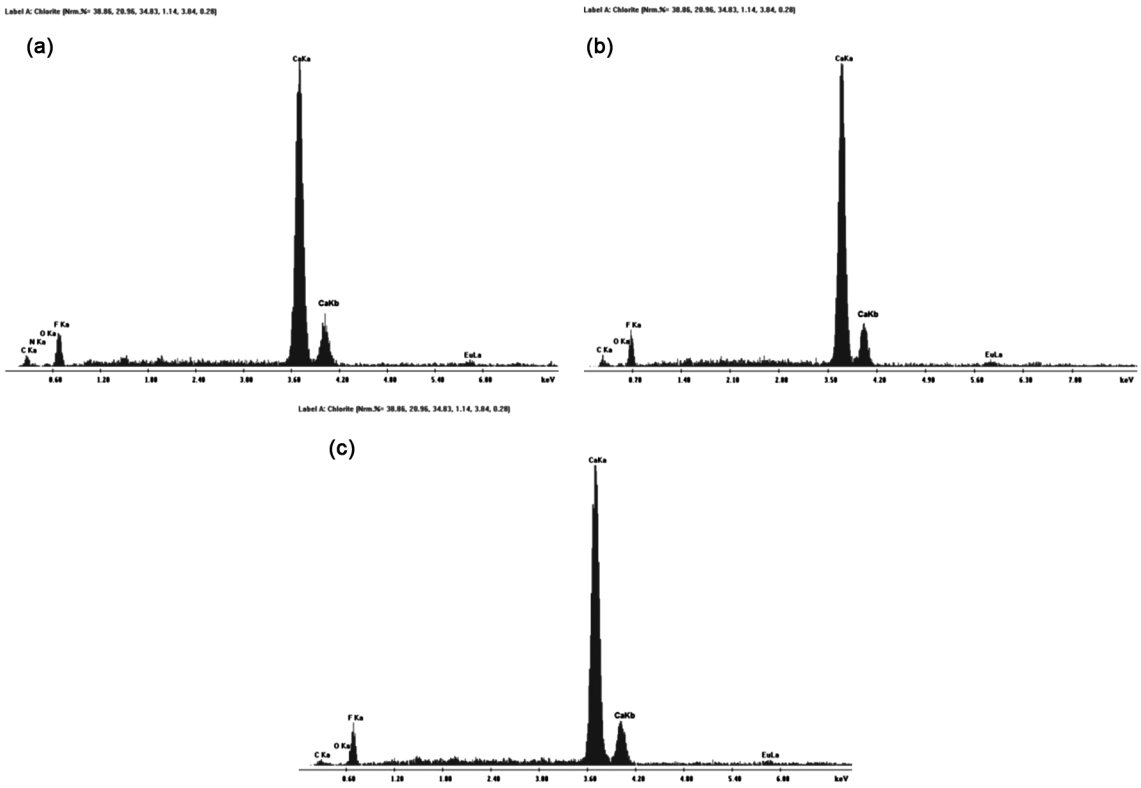

Fig. 3 — EDX spectra of (a) CF_EDTA, (b) CF_TSC and (c) CF_EG NPs sample

The room temperature fluorescence properties of the synthesized NPs were investigated using photo-luminescence excitation and emission spectra recorded at an emission and excitation wavelengths of 591 nm and 394 nm respectively. In Fig. 5(a), the excitation spectra consist of bands at 318, 361, 380 and 394 nm respective to the $^7F_0 \rightarrow {}^5H_{3,6}$, $^7F_{0,1} \rightarrow {}^5D_0$, $^7F_{0,1} \rightarrow {}^5G_1$ and $^7F_0 \rightarrow {}^5L_6$ transitions of Eu^{3+} (Ref. 30). In the spectra, the peak intensity increases when the capping ligand of the samples changes from EDTA to citrate through ethylene glycol indicating the important role played by the different capping ligands. The variation is attributed to the extent of defects acquired during the growth of the particles as well as the varying degree of dangling bonds introduced onto the surface of the NPs by the different ligands.

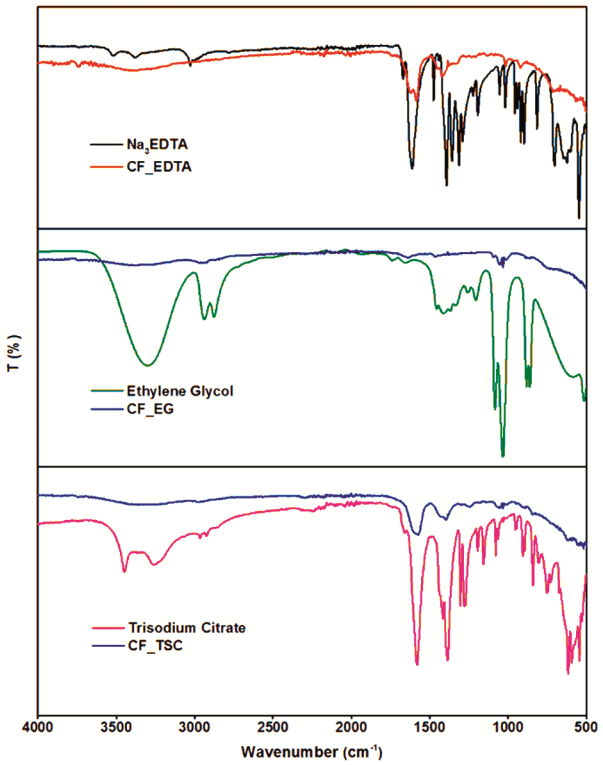

Fig. 4 — FT-IR spectra of the synthesized NPs samples of CF_EDTA, CF_EG and CF_TSC along with the spectra of trisodium salt of ethylenediamminetetraacetic acid (Na_3EDTA), ethylene glycol and trisodium citrate indicated by different colours

The emission spectra in Fig. 5(b) shows characteristic bands of Eu^{3+} positioned at 591, 615, 650 and 692 nm originating from $^5D_0 \rightarrow {}^7F_1$, $^5D_0 \rightarrow {}^7F_2$, $^5D_0 \rightarrow {}^7F_3$ and $^5D_0 \rightarrow {}^7F_4$ transitions respectively out of which the peaks at 591 and 615 nm dominated. These two transitions namely $^5D_0 \rightarrow {}^7F_1$ and $^5D_0 \rightarrow {}^7F_2$ are magnetic and electric dipole transitions in which the first is allowed by the Laporte Selection rule while the later is forbidden. The rule strictly applies to a centrosymmetric gaseous lanthanide ion but for the ions embedded in a matrix, it is relaxed due to coupling with vibrational states or mixing of higher configurations with the 4f wavefunctions caused by a crystal field. Consequently, the intensity of $^5D_0 \rightarrow {}^7F_1$ transition is largely independent of Eu^{3+} ion environment while for $^5D_0 \rightarrow {}^7F_2$ transition, a symmetric environment will lower the intensity and an asymmetric local environment will enhance its intensity, due to which the latter is referred to as hypersensitive transition. In the spectra, the intensity of $^5D_0 \rightarrow {}^7F_1$ transition of the NP samples increases in the order CF_EDTA < CF_EG < CF_TSC which is similar with the trend in excitation spectra, while the increase for $^5D_0 \rightarrow {}^7F_2$ transition follows: CF_EG < CF_TSC < CF_EDTA.

Since the hypersensitive transition is responsible for the typical red luminescence, a comparison of its intensities among NPs samples stabilized by different ligands will reveal the important roles played by the ligands in enhancing the red component of the emitting light. The ratio *R*, defined by $I(^5D_0 \rightarrow {}^7F_2)/I(^5D_0 \rightarrow {}^7F_1)$ is used to compare the intensities of the

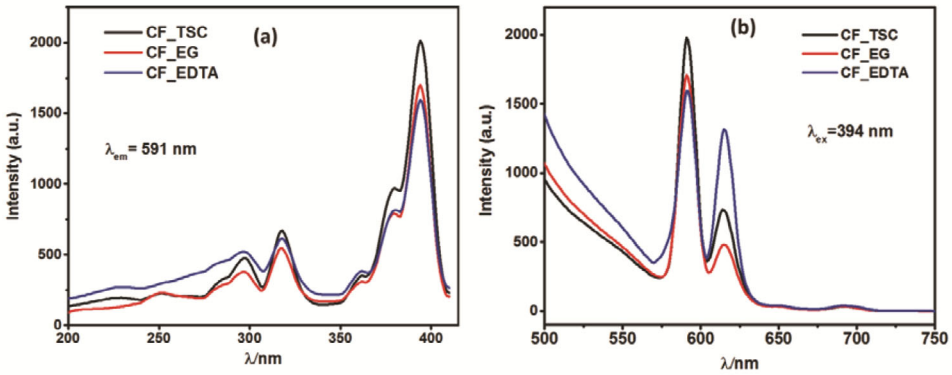

Fig. 5 — (a) Excitation spectra monitored at λ_{em}=591 nm and (b) emission spectra at λ_{ex}=394 nm of CF_TSC, CF_EG and CF_EDTA NPs

hypersensitive transitions of different samples. Table 2 lists the values of *R*, Judd-Ofelt intensity parameter (Ω_2), and radiative transition probalilities (*A*) for $^5D_0 \rightarrow {}^7F_2$ transitions of the three NP samples. The method for calculating Ω_2 and *A* is described elsewhere[31]. Intensities of the hypersensitive transition of Eu^{3+} are described by and proportional to Ω_2 parameter. The *R* values indicate greater number of Eu^{3+} occupies the Ca^{2+} sites as compared to those in the defect lattice or the grain boundary for all the NP samples. All the samples have Ω_2 parameters comparable to Eu^{3+} (aq) ion (1.62×10^{-20} cm^2) (Ref. 32). Among the three NP samples, CF_EDTA have the largest *R* and Ω_2 parameter which translate to the $^5D_0 \rightarrow {}^7F_2$ emission intensity of more than double the intensity of CF_EG and one-half of that of CF_TSC. Although, the trend, which is also supported by the radiative transition probabilities, is in agreement with XRD analysis where the magnitude of the strain values (Table 1) increases when ligand changes from EG to EDTA through TSC; it is not the symmetry of the Eu^{3+} site alone that depicts the *R* values but also the nature of the ligands/anions as in the case of many Eu^{3+} complexes/compounds[31,9]. For NPs, binding of Eu^{3+} with ligands take place only on the surface, so the Eu^{3+} sites at the grain boundary make significant contribution to the intensity of the electric dipole transition apart from those in the lattice defects. It is the cumulative effect of the contributions of emitting sites from both the lattice defects as well as the grain boundary that resulted in the variation of emission intensities for different NP samples. Among the stabilizing agents, EG does not form chemical bonds with either Ca^{2+} or Eu^{3+} (Ref. 28) while TSC and EDTA form complexes with Eu^{3+} because of which the later two ligands were able to create a more asymmetric environment around Eu^{3+} sites at the grain boundary. Also, the higher many body effect in the binding pocket of EDTA contributes larger to the polarizability of the ligand as compared to TSC which has only three acetate groups[33,34]. All these factors combined with the lattice strain resulted in the enhancement of emission intensity of hypersensitive transition by EDTA to the maximum and by EG to the minimum.

The emission decay curves (Fig. 6) of $^5D_0$ level of Eu^{3+} of all the samples monitored at 591 nm emission and 394 nm excitation shows a biexponential decay behavior which can be fitted in equation (1)[35]. In the equation, τ_1 and τ_2 are two fluorescence lifetimes and A_1 and A_2 are amplitude fractions obtained as fitting parameters.

$$I = A_1\left(e^{-t/\tau_1}\right) + A_2\left(e^{-t/\tau_2}\right) \quad (1)$$

The intensity average lifetimes were determined using the following equation:

$$I = \frac{A_1\tau_1^2 + A_2\tau_2^2}{A_1\tau_1 + A_2\tau_2} \quad (2)$$

Table 3 presents the fitting parameters and the average lifetimes of the NP samples which verify the

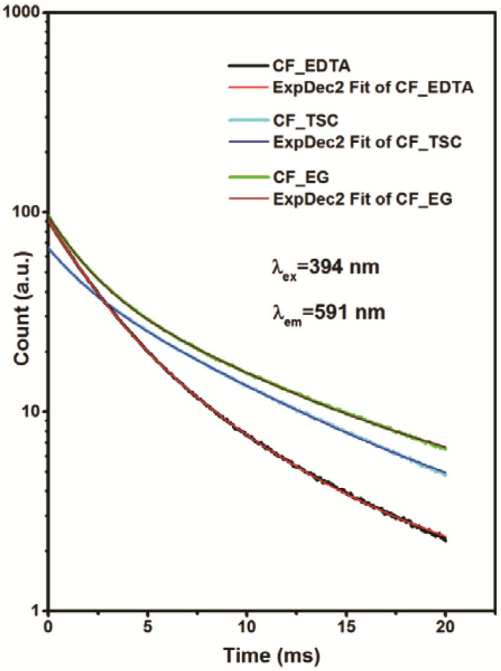

Fig. 6 — Luminescence decay curves of CaF_2:3Eu NPs stabilized by EDTA, TSC and EG monitored at 591 nm emission and 394 nm excitation fitted with biexponential decay

Table 2 — The calculated asymmetric ratio (R), the Judd-Ofelt intensity parameter (Ω_2) and the radiative transition probability (A) for $^5D_0 \rightarrow {}^7F_2$ transition of CF_EDTA, CF_TSC and CF_EG NPs

Samples	*R*	$\Omega_2/10^{-21}$ (cm^2)	A(J=0,J′=2) (s^{-1})
CF_EDTA	0.755879646	12.5011	32.31195695
CF_TSC	0.501076098	8.23755	21.37192476
CF_EG	0.381206327	6.28875	16.27333063

Table 3 — Luminescence decay parameters derived from bi-exponential fitting

Samples	τ_1	τ_2	A_1	A_2	τ_{av}	R^2_{adj}
CF_EDTA	1.44854±0.01	4.20813±0.03	58.15344±0.34	30.82465±.32	3.12	0.99998
CF_TSC	1.23134±0.01	5.38282±0.2	21.91373±0.15	42.29751±0.13	4.94	0.99995
CF_EG	5.52573±0.03	1.19242±0.01	43.49042±0.14	48.66889±0.16	4.68	0.99996

τ_1 and τ_2 are different lifetimes; τ_{av} is average lifetime; A_1 and A_2 are amplitude fractions; R^2_{adj} shows the goodness of fitting.

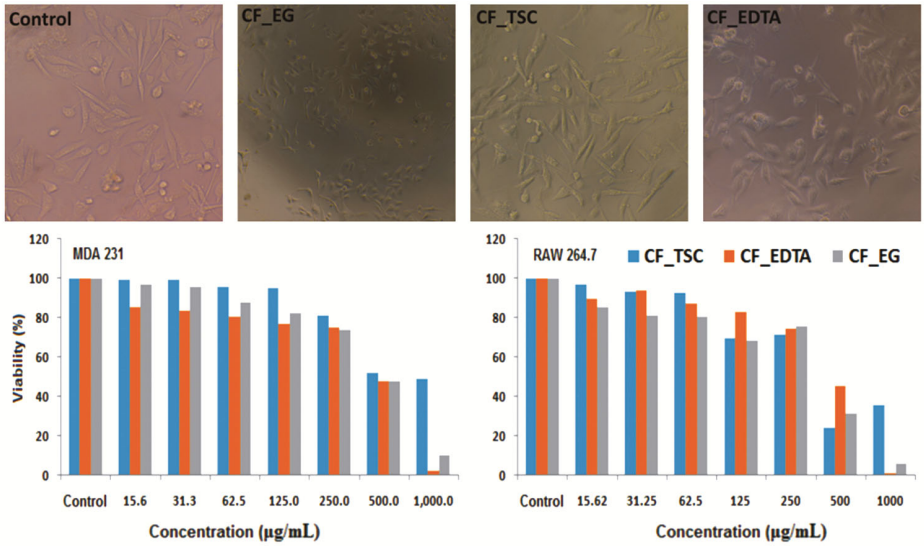

Fig. 7 — Top panel: Representative microscopic images of MDA 231 cells incubated with CF_EG, CF_TSC, CF_EDTA and control for 24 hr; bottom panel: percentage cell viability of MDA 231 and RAW 264.7 cells treated with CF_TSC, CF_EDTA and CF_EG NPs at varying concentrations

significance of stabilizing ligands on the luminescence properties of the NPs. The occurrence of two distinct lifetimes further confirmed the existence of Eu^{3+} in two different environments as discussed earlier. The contributions of Eu^{3+} present in the grain boundary to the average lifetimes increases in the order: CF_EG < CF_TSC < CF_EDTA.

The applicability of the synthesized NPs samples in biological studies was assessed with MTT analysis in both normal and cancer cells. Fig. 7 (top panel) shows the microscopic images of MDA 231 cells incubated with 250 µg/mL concentration of CF_EG, CF_TSC and CF_EDTA samples for 24 h along with the cells alone (control). The bottom panel is the graphical representations of the results of MTT assay carried out on MDA 231and normal RAW 264.7 cell lines with varying concentrations (1000, 500, 250, 125, 62.5, 31.2 and 15.6 µg/mL). The results inferred that the cells remained morphologically intact upto a NPs concentration 250 µg/mL with a viability of around 75% for all the samples. Some reports showed 80% viability at 1 mM (Ref. 8), 75% viability at 100 µg/mL (Ref. 36), *etc*.

The ability of the stabilizing ligands of the synthesized NPs to bind with bovine serum albumin (BSA) was studied by fluorometric assay. When excited at 280 nm, BSA shows emission at 339 nm which is subsequently quenched with the addition of increasing amounts of NP samples due to the binding between the two entities as is represented in Fig. 8. The binding constant, K_b can be determined from the

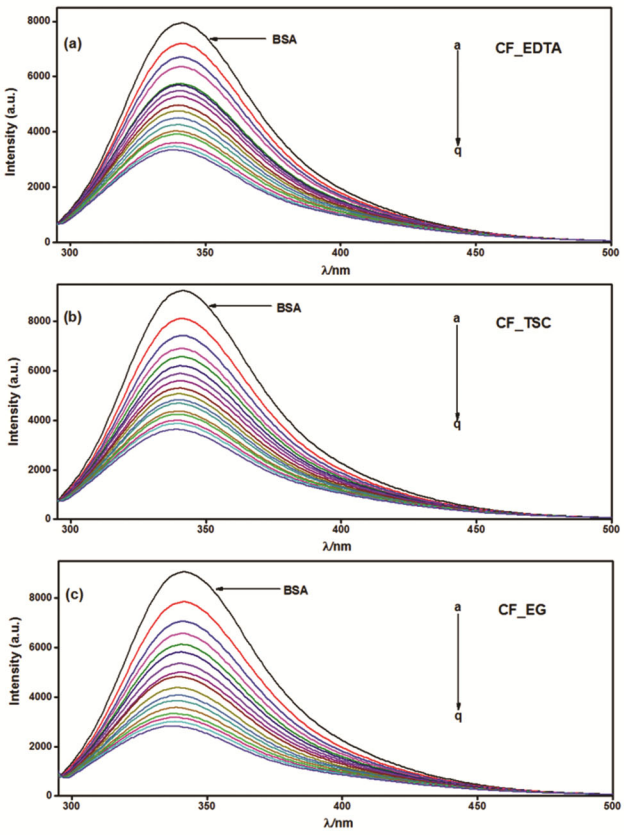

Fig. 8 — Emission spectra of BSA (3×10^{-5} mol dm^{-3}) with (a) CF_EDTA, (b) CF_TSC and (C) CF_EG at various NPs concentrations – a) 0, b) 1.4×10^{-4}, c) 2.9×10^{-4}, d) 4.3×10^{-4}, e) 5.7×10^{-4}, f) 7.2×10^{-4}, g) 8.6×10^{-4}, h) 10.1×10^{-4}, i) 11.5×10^{-4}, j) 12.9×10^{-4}, k) 14.3×10^{-4}, l) 15.8×10^{-4}, m) 17.2×10^{-4}, n) 18.6×10^{-4}, o) 20.0×10^{-4}, p) 21.4×10^{-4} and q) 22.8×10^{-4} mol dm^{-3}

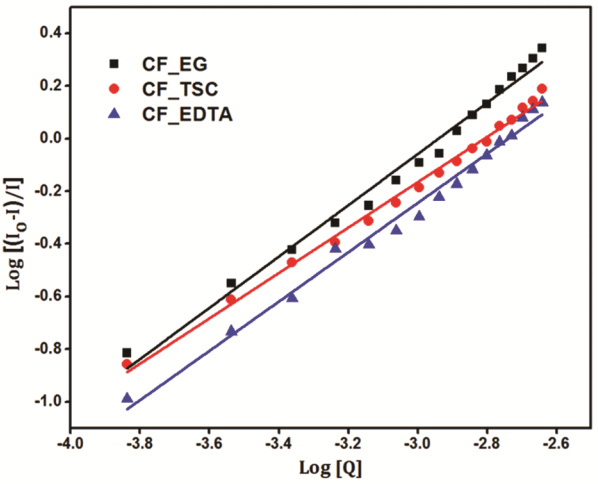

Fig. 9 — Double logarithmic plot for binding BSA with a) CF_EG, b) CF_TSC and c) CF_EDTA NPs

double logarithmic plot of $\log[(I_o\text{-}I)/I]$ *vs*. log[Q] (Fig. 9) utilizing the double logarithmic regression equation[27] (eqn 3).

$$\log\left[\frac{I_o - I}{I}\right] = \log K_b + n \log [Q] \quad (3)$$

where, I_o and I are the emission intensity of BSA in the absence and presence of a certain concentration of quencher [Q] which in our case is the synthesized NPs, K_b is the binding constant and n is the average binding number. The calculated values of K_b for binding BSA with CF_EG, CF_TSC and CF_EDTA are 7.27×10^2 dm^3 mol^{-1}, 2.62×10^2 dm^3 $mol^{-1}$and 3.66×10^2 dm^3 mol^{-1} respectively. Using the K_b values obtained, the free energy changes for the binding of NPs with BSA were computed using equation (4).

$$\Delta G = -2.303\, RT \log K_b \quad (4)$$

where, ΔG is free energy change, K_b is binding constant, R is the universal gas constant and T is the temperature. ΔG values associated with the binding of BSA with CF_EG, CF_TSC and CF_EDTA are respectively –16.32 kJ mol^{-1}, –13.80 kJ mol^{-1} and –14.62 kJ mol^{-1} suggesting a spontaneous binding process.

Conclusions

Enhancement of the intensity of hypersensitive $^5D_0 \rightarrow {}^7F_2$ transition of Eu^{3+} emission in Eu(III) doped CaF_2 NPs can be achieved by choosing appropriate capping ligands among the most common and easily available stabilizing agents - EG, TSC and EDTA. A low doping concentration made a very little compromise in the crystallinity of the NPs, although the different binding capabilities of the ligands results in the introduction of varying extent of defects during the growth of the particles. EDTA capped NPs has the largest R and Ω_2 values followed by NPs stabilized by TSC and EG. Significant contribution from the Eu^{3+} sites at the grain boundary combined with those occupying the defect sites resulted into the observed variation in the intensity of $^5D_0 \rightarrow {}^7F_2$ transition. In addition to the asymmetric environment of the Eu^{3+} at the grain boundary, the polarizability of the stabilizing ligands bound to it on the surface of NPs positively contribute to the enhancement of the intensity. EDTA being the maximum polarisable ligand coupled with the highest micro-strain of the particle manifests the maximum enhancement. All the NPs samples show cytofriendly nature with human breast cancer cells (MDA 231) as well as RAW 264.7 cells upto a fairly high concentration of 250 µg/mL with a viability of around 75%. Emission titration study of the binding of the NP samples to BSA reveals the process to be spontaneous with a fair value of binding constants. All these results point to the fact that the enrichment of the red component of Eu^{3+} spectrum in Eu^{3+} doped CaF_2 can simply be achieved by choosing the appropriate ligands at comparatively low dopant concentration for the purpose of bioimaging and other bioapplications.

Acknowledgements

The authors are grateful to Heisnam Rameshwari Devi and Dr. Nanaocha Sharma of Institute of Bioresources and Susainable Development Imphal for cytotoxicity studies.

References

1 Kawano K, Arai K, Yamada H, Hashimoto N & Nakata R, *Sol Ene Mat Sol Cells*, 48 (1997) 35.
2 Bouzigues C, Gacoin T & Alexandrou A, *ACS Nano*, 5 (2011) 8488.
3 Iwanaga H, *Materials*, 3 (2010) 4080.
4 Hussain R, Kruk S S, Bonner C E, Noginov M A, Staude I, Kivshar Y S, Noginova N & Neshev D N, *Opt Lett*, 40 (2015) 1659.
5 Parchur A K & Ningthoujam R S, *RSC Adv*, 2 (2012) 10859.
6 Bondzior B & Dereń P J, *J Lumin*, 201 (2018) 298.
7 Liu Y, Gou H, Huang X, Zhang G, Xi K & Jia X, *Nanoscale*, 12 (2020) 1589.
8 Sasidharan S, Jayasree A, Fazal S, Koyakutty M, Nair S V & Menon D, *Biomat Sci*, 1 (2013) 294.
9 Srivastava A M, Brik M G, Beers W W, Ma C G, Piasecki M & Cohen W E, *J Lumin*, 257 (2023) 119709.
10 Shen J, Sun L D & Yan C H, *Dalton Trans*, 14 (2008) 5687.
11 Escribano P, Julian-Lopez B, Planelles-Arago J, Cordoncillo E, Vianab B & Sanchez C, *J Mater Chem*, 18 (2008) 23.

12 Quan Z, Yang D, Yang P, Zhang X, Lian H, Liu X & Lin J, *Inorg Chem*, 47 (2008) 9509.
13 Bensalaha A, Mortiera M, Patriarcheb G, Gredinc P & Viviena D, *J Solid State Chem*, 179 (2006) 2636.
14 Maushake P, *Optik & Photonik*, 3 (2008) 46.
15 Chithrani B D, Ghazani A A & Chan W C W, *Nano Lett*, 6 (2006) 662.
16 Gratton S E A, Ropp P A, Pohlhaus P D & DeSimone J M, *Pro Nat Acad Sci*, 105 (2008) 11613.
17 Wu M, Guo H, Liu L, Liu Y & Xie L, *Int J Nanomed*, 14 (2019) 4247.
18 Goldburt E T, Kulkani B, Bhargava R N, Taylor J & Libera M, *Mater Res Soc Symp Proc*, 424 (1996) 441.
19 Goldburt E T, Kulkani B, Bhargava R N, Taylor J & Libera M, *J Lumin*, 72–74 (1997) 190.
20 Ningthoujam R S, *In Synthesis*, *Characterization and Applications of Multifunctional Materials*, (Nova Science Publishers Inc., Hauppauge, NY) 2012, p. 145.
21 Wakefield G, Keron H A, Dobson P J & Hutchison J L, *J Colloid Interface Sci*, 215 (1999) 179.
22 Ritter B, Haida P, Fink F, Krahl Z, Gawlitza K, Rurack K, Scholz G & Kemnitz E, *Dalton Trans*, 46 (2017) 2925.
23 Song L & Xue L, *Appl Surf Sci*, 258 (2012) 3497.
24 Cho S, Park S J, Ko S Y, Park J & Park S, *Biomed Microdev*, 14 (2012) 1019.
25 Sousa S M G, Bramante C M & Taga E M, *Braz Dent J*, 16 (2005) 3.
26 Cortelletti P, Pedroni M, Boschi F, Pin S, Ghigna P, Canton P, Vetrone F & Speghini A, *Cryst Growth Des*, 18 (2018) 686.
27 Sharma A S, Anandakumar S & Ilanchelian M, *R S C Adv*, 4 (2014) 36267.
28 Singh NB, Devi TC & Singh TD, *Russ. J. Inorg. Chem*., 68 (2023) 1690.
29 O'Brien L C, Root H B, Wei C, Jensen D, Shabestary N, Meo C D & Eder D J, *J Chem Educ*, 92 (2015) 1547.
30 Luwang M N, Ningthoujam R S, Jagannath, Srivastava S K & Vatsa R K, *J Am Chem Soc*, 132 (2010) 2759.
31 Binnemans K, *Coord Chem Rev*, 295 (2015) 1.
32 Binnemans K, Herck K V & Görller-Walrand C, *Chem Phys Lett*, 266 (1997) 297.
33 Mason S F, Peacock R D & Stewart B, *Mol Phys*, 30 (1975) 1829.
34 Jing Z, Liu C, Qi R & Ren P, *Proc Natl Acad Sci*, 115 (2018) 7495.
35 Sillen A & Engelborghs Y, *Photochem Photobiol*, 67 (1998) 475.
36 Singh L P, Srivastava S K, Mishra R & Ningthoujam R S, *J Phys Chem C*, 118 (2014) 18087.